INTERNATIONAL JOURNAL OF HYDROGEN ENERGY 44 (2019) 8479–8492

Available online at www.sciencedirect.com

ScienceDirect

journal homepage: www.elsevier.com/locate/he

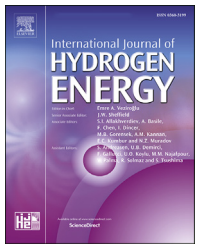

Power management system for a fuel cell/battery hybrid vehicle incorporating fuel cell and battery degradation

Yongqiang Wang [a], Scott J. Moura [b], Suresh G. Advani [a], Ajay K. Prasad [a,*]

[a] Center for Fuel Cells and Batteries, Department of Mechanical Engineering, University of Delaware, Newark, DE, 19716, USA

[b] Department of Civil and Environmental Engineering, University of California, Berkeley, CA 94720, USA

ARTICLE INFO

Article history:
Received 7 December 2018
Received in revised form
29 January 2019
Accepted 3 February 2019
Available online 28 February 2019

Keywords:
Power management
Durability
Hybrid vehicle
PEMFC
ECSA
Lithium-ion battery

ABSTRACT

Optimization of fuel cell/battery hybrid vehicle systems has primarily focused on reducing fuel consumption. However, it is also necessary to focus on fuel cell and battery durability as inadequate lifespan is still a major barrier to the commercialization of fuel cell vehicles. Here, we introduce a power management strategy which concurrently accounts for fuel consumption as well as fuel cell and battery degradation. Fuel cell degradation is quantified using a simplified electrochemical model which provides an analytical solution for the decay of the electrochemical surface area (ECSA) in the fuel cell by accounting for the performance loss due to transient power load, start/stop cycles, idling and high power load. The results show that the performance loss based on remaining ECSA matches well with test data in the literature. A validated empirical model is used to relate Lithium-ion battery capacity decay to C-rate. Simulations are then conducted using a typical bus drive cycle to optimize the fuel cell/battery hybrid system. We demonstrate that including these degradation models in the objective function can effectively extend the lifetime of the fuel cell at the expense of higher battery capacity decay resulting in a lower average running cost over the lifetime of the vehicle.

Introduction

Electric vehicles powered by lithium-ion batteries have been gaining ground over conventional Internal Combustion (IC) Engine vehicles in recent years as a viable solution to combat global warming caused by excessive use of fossil fuels. Despite promising progress, the lithium-ion battery continues to present concerns regarding its durability, recharging time and especially driving range as compared to IC engines [1,2]. On the other hand, fuel cell vehicles operating on hydrogen have the advantage of refueling time and driving range comparable to fossil fuel vehicles [3]. As a result, major automakers are now competing to release fuel cell vehicles on the market. Most of these vehicles are equipped with a relatively large load-following fuel cell stack coupled with a small battery. For example, the Toyota Mirai is equipped with a 113 kW fuel cell stack and a 1.6 kWh Nickel-metal hydride battery pack [4].

* Corresponding author.
E-mail addresses: sailor@udel.edu (Y. Wang), smoura@berkeley.edu (S.J. Moura), advani@udel.edu (S.G. Advani), prasad@udel.edu (A.K. Prasad).

https://doi.org/10.1016/j.ijhydene.2019.02.003
0360-3199/

These powertrain configurations are intended to let the fuel cell stack provide the majority of the power demand and use the battery merely as a buffering device for high transient power demand. Different power management strategies usually result in different load cycles which could significantly affect the lifetime of the fuel cell stack. It is thus important to understand the degradation mechanisms of the fuel cell stack and improve its durability by accounting for those mechanisms into the power management system.

The Center for Fuel Cell and Batteries at the University of Delaware has been conducting a Fuel Cell Hybrid Bus Program since 2005 to research, build and demonstrate fuel cell powered buses and hydrogen refueling station in Newark, Delaware [5]. While equipped with a sophisticated powertrain, most fuel cell hybrid vehicles use a rule-based power management strategy due to its simplicity and ease of implementation [6,7]. Similarly, our buses use a rule-based power management strategy which is designed to turn on the fuel cell at its optimal efficiency point to meet the predicted energy requirement during a specific drive cycle. This approach was validated with the UD fuel cell buses on campus to provide better fuel economy [8]. The parameters used in this paper are based on drive cycle data collected from our latest bus equipped with a 58 kW fuel cell stack (three Ballard Mark 9 SSL fuel cell stacks, each rated at 19.4 kW) and a 25 kWh lithium-ion battery (XALT 75 Ah High Power (HP) Superior Lithium Ion Cell). The fuel cell system consists of the fuel cell stack, hydrogen tank, air compressor and cooling system. The stack is connected in parallel with the battery system through a boost converter to match the high voltage of the battery which powers an AC induction motor through an inverter. The powertrain of the bus is shown in Fig. 1.

The power management strategy introduced in this paper includes a physical degradation model of the electrochemically active surface area (ECSA) of the fuel cell, as well as a model for battery capacity decay. To the best knowledge of the authors, this is the first time that a physical model of ECSA degradation is directly integrated into the power management strategy to improve the durability of the fuel cell stack and hence improve the commercial viability of fuel cell vehicles. This framework can allow for the inclusion of other fuel cell degradation mechanisms as and when such physical degradation models become available. This ultimately enables control designs that intelligently avoid adverse operating conditions and improve the lifetime of fuel cell stacks.

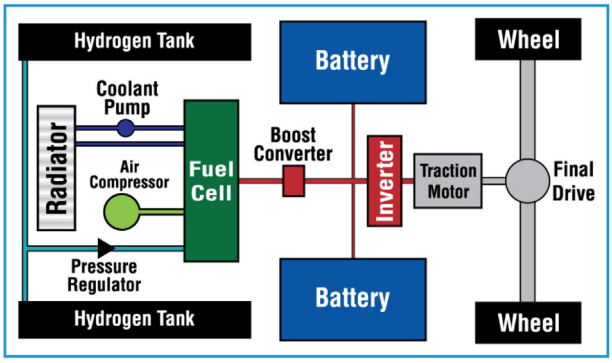

Fig. 1 – Powertrain of the University of Delawares fuel cell/battery hybrid bus.

This paper is organized as follows. The degradation mechanisms of the fuel cell stack and lithium-ion battery are introduced in the next section. This is followed by a detailed description of the numerical models and validation of the performance drop caused by ECSA decay, and the resulting polarization curve of the fuel cell stack. A model for the battery capacity fade is then introduced and coupled with the fuel cell degradation model into the final cost function for optimal control. The results from the simulations are discussed next, and we summarize our main findings in the conclusion section.

Degradation of the fuel cell and battery

Fuel cell degradation is a complex process that consists of many different mechanisms ranging from electrochemical to mechanical degradation [9–12]. Among them, catalyst degradation contributes significantly to fuel cell performance loss over time [13]. Specifically, the loss of ECSA within the catalyst layer structure strongly affects fuel cell performance [14–16]. Experimental data in Ref. [17] showed that the kinetic performance losses can be attributed to the loss of ECSA over time. Two operating conditions principally contribute to ECSA loss. The first is high potential under which the Platinum(Pt) catalyst nanoparticles undergo high dissolution rates followed by redeposition and particle agglomeration [18–21]. The other is reactant starvation [22] which often occurs during the startup/shutdown process and transient power loading when the reactant supply is insufficient [23–25]. This causes high overpotential which accelerates the corrosion of the carbon support of Pt particles. Both effects cause small Pt particles to agglomerate due to their higher free energy and thus reduce the ECSA and hence the performance. High current density can also accelerate Pt particle agglomeration [26] and thus speed up ECSA decay. ECSA decay directly increases the activation loss of the fuel cell. It can also increase mass transfer loss mainly due to the increased oxygen transfer resistance caused by smaller reaction sites [27]. The high oxygen transport resistance is usually measured using the limiting current method [28] and is often associated with low Pt-loading fuel cells [29–31]. It was shown in Ref. [27] that performance loss associated with the increase of oxygen transfer resistance caused by ECSA loss is twice the activation loss under high current density (1.7 A/cm^2).

Due to the complexity of the degradation mechanisms mentioned above, most degradation models developed for transient applications are empirical. Theoretical models are usually developed to explain laboratory results for a specific degradation mechanism [11]. For example, a chemical membrane degradation model coupled with cell performance was developed [32] to simulate voltage degradation which showed good agreement with the experimental data under open circuit voltage (OCV) hold. Reference [33] modeled the degradation of the fuel cell by fitting parameters to the polarization curve obtained from experiments. Reference [34] built a lifetime model of the fuel cell stack based on the characteristics

of the current and voltage profiles for different operating cycles. References [35,36] performed a set of experiments to isolate the performance decay caused by transient operating conditions for a bus application and separated their corresponding contributions to the performance decay of the fuel cell stack. Finally [37], coupled a degradation model of membrane conductivity using a static degradation library with a physical fuel cell model that solves for the local potential, reactant concentration and pressure in the channel, etc. to study the lifetime of the fuel cell stack under a repeated drive cycle. They showed a lifetime exceeding 6555 h for a pure fuel cell vehicle. However, this framework might not be suitable for power management studies due to the extreme computational burden of considering so many physical states in the fuel cell model.

In this paper, we focus on one of the main degradation mechanisms of fuel cells, which is the degradation of the Pt catalyst. Among the theoretical models concerning ECSA loss caused by Pt degradation [38], developed a comprehensive ECSA decay model based on platinum dissolution under different potential holds and the results agree well with the experimental data from Refs. [18–20]. This model is particularly useful because it gives the ECSA decay rate under different high potentials which corresponds to the performance decay data under idling conditions from Ref. [35]. This means we can effectively convert other degradation mechanisms typically found in transient load cycles into ECSA decay and calculate the detailed reduction in stack performance over its lifetime. This results in a more dynamic and accurate representation of the degradation of the fuel cell stack throughout its lifetime.

The literature contains many efforts to improve the fuel economy and durability of fuel cell/battery hybrid vehicles. For example, references [39,40] conducted a parametric study by considering transient power demand on the fuel cell stack using convex optimization. Both studies show that the resulting power demand on the fuel cell stack still suffers from rapid fluctuation due to a lack of hard constraints on the transient power variation. Reference [41] employed a Pontryagin Minimum Principle (PMP) based optimization procedure to prolong fuel cell lifetime by including transient power load in the controller based on the lifetime model derived from Ref. [35]. Reference [42] studied the cost and greenhouse gas emission over the lifetime of the fuel cell stack in passenger cars subjected to real-world drive cycles, and concluded that fuel cell vehicles are becoming more viable. The voltage degradation rate reported in Ref. [36] was used to model the fuel cell degradation in Ref. [42]. The same fuel cell performance decay model and battery capacity fade model used in this paper were used directly in Ref. [43] to convert degradation cost to equivalent hydrogen consumption cost which was then included in energy management optimization to reduce life cycle cost. A recent paper [44] also tried to improve fuel cell lifetime by including degradation terms associated with high and low power levels, transient power, and start/stop cycles in the controller. These factors were provided by the manufacturer and the results showed that the lone startup/shutdown during the entire cycle dominates degradation. All these models tend to incorporate degradation mechanisms based solely on empirical data, or specific models which might not translate well to alternate system configurations. The model developed in this paper bridges this gap and converts empirical models into corresponding physical degradation models that could be applied to any system configuration.

Models concerning the degradation of lithium-ion batteries range from first principle simulations [45] which account for the solid electrolyte interphase (SEI) growth and resulting capacity loss, to empirical data-fitting [46] which represents capacity fade as a function of C-rate. The determining factor for battery capacity decay is still the Ah throughput which is used in this paper to implement the aging model from Ref. [46].

Simulation model

This section describes the degradation models used in this study and the formulation of the optimization strategy.

Fuel cell degradation model based on ECSA loss

The ECSA decay and its deleterious effects on the polarization curve are modeled in this section.

ECSA degradation model

ECSA degradation is based on the platinum dissolution model provided by Ref. [38] in which the full set of electrochemical equations was simplified to a single continuity equation:

$$\frac{\partial f(\xi,\tau)}{\partial t}+\xi^2 exp(\xi)\frac{\partial f(\xi,\tau)}{\partial \xi}=-\xi^2 exp(\xi) f(\xi,\tau) \tag{1}$$

where $f(\xi,\tau)$ is the platinum particle radius distribution (PRD) function, and ξ and τ are nondimensional variables:

$$\tau=\frac{t}{T_0} \text{ and } \xi=\frac{R_0}{r} \tag{2}$$

in which the characteristic time and radius are defined by:

$$T_0=\frac{2\beta_t\gamma_{Pt}}{RTk_{Pt}^{\infty}} \text{ and } R_0=\frac{2\beta_t\gamma_{Pt}\overline{V}_{Pt}}{RT} \tag{3}$$

Here, the transfer coefficient β_t and surface tension γ_{Pt} are combined to represent the effective surface tension. Parameter k_{Pt}^{∞} is the effective bulk rate constant for Pt–O dissolution and $\overline{V}_{Pt}$ is the molar volume of Pt ($9.1\times10^{-6}\ m^3/mol$).

The values of effective surface tension $\beta_t\gamma_{Pt}$ and k_{Pt}^{∞} were derived from curve-fitting the ECSA degradation model with in situ test results of ECSA change under constant potential hold at 0.75 V and 0.95 V in Ref. [18]. These authors also confirmed that the predicted effective surface tension ratio from their model was comparable to the experimental ratio for friction coefficients at 0.75–0.95 V from Ref. [47], which indicated that the coefficient of friction was indeed proportional to the surface tension as suggested in Ref. [47]. Since [47] also showed that the coefficient of friction was proportional to the potential between 0.7 and 0.95 V, we assumed that the effective surface tension should also be linearly related to the potential. Thus, the values of $\beta_t\gamma_{Pt}$ in Ref. [38] are linearly extrapolated to estimate the value of $\beta_t\gamma_{Pt}$ between 0.7 and 0.95 V.

The Pt dissolution rate k_{Pt}^{∞} was also empirically modeled [38] as:

$$k_{Pt}^{\infty} = k_{Pt}^{w} = \lambda\theta_{PtO} exp\left(\frac{w\theta_{PtO}}{RT}\right) \quad (4)$$

where λ is a parameter collecting all the potential-independent factors. w is the interaction energy ($w = 24$ kJ/mol). θ_{PtO} is the PtO coverage in percentage which is estimated to be 0.4 at 0.75 V and 1 above 0.95 V. Parameter θ_{PtO} is also shown to be linearly proportional to potential between 0.6 and 1.2 V in Ref. [48]. Thus, the value of θ_{PtO} is also extrapolated between 0.7 and 0.95 V based on the values at 0.75 V and 0.95 V in Ref. [38]. Parameter θ_{PtO} is assumed to be 0 below 0.7 V.

The governing equation Eq. (1) can be solved implicitly in terms of two equations [38]:

$$f(\xi,\tau) = f_0(\xi_0) exp(-(\xi - \xi_0)) \quad (5)$$

and

$$-\frac{exp(-\xi)}{\xi} + Ei(1,\xi) = \tau - \frac{exp(-\xi_0)}{\xi_0} + Ei(1,\xi_0) \quad (6)$$

where ξ_0 is a parametric variable and $f_0(\xi_0)$ is the initial particle radius distribution parametrized by ξ_0. $Ei(1,\xi_0)$ is the exponential integral function of ξ_0. The ECSA change over the lifetime of the fuel cell can then be calculated by solving Eqs. (5) and (6).

Based on the assumption that the effective surface tension term $\beta_t\gamma_{Pt}$ and platinum surface coverage θ_{PtO} are linearly dependent on potential between 0.7 and 0.95 V, $\beta_t\gamma_{Pt}$ and k_{Pt}^{∞} are interpolated based on the fitted values provided by Ref. [38]. The ECSA decay under different potentials is calculated and shown in Fig. 2a. Not surprisingly, the ECSA under low potential of 0.7 V only drops by 50% after 5000 h, which is the average lifetime observed in most of the previous studies relating to automotive fuel cells [49]. For high potential hold of 1 V, the ECSA drops rapidly by about 90% after just 2000 h. This shows that the operating potential has a significant effect on the ECSA decay rate. The ECSA decay rate is then extracted from the degradation model as shown in Fig. 2b. It is assumed that the ECSA decay rate is only a function of potential. This can be justified by assuming that the fuel cell operates under relatively stable power levels most of the time, whereas the electrochemical process is much faster (usually in the sub-second domain). Also, the ECSA decay rate derived here is only for low power or idling operating conditions which usually does not involve much power fluctuation. Therefore, we can assume that the Pt dissolution process reaches a stable equilibrium at any given time, and thus the ECSA decay rate is only a function of fuel cell voltage.

The real-time fuel cell power can change fairly quickly for a given drive cycle. Solving the implicit equations in Eq. (1) and corresponding ECSA decay rate at every single timestep would be very time-consuming to implement in an optimization strategy. To address this challenge, a pseudo load profile was simulated to determine whether it is reasonable to substitute the weighted time average of the final PRD under different potentials for the actual final PRD after a certain time period of the drive cycle. The chosen profile is 550 h long during which the fuel cell operates under different potentials from 0.7 V to 0.95 V for various time periods. Given the same initial PRD, the final PRD is calculated either by directly solving Eq. (1) at each timestep, or by computing the weighted average of the final PRD function under different potentials based on the cumulative duration of fuel cell operation under each potential. The simulation results shows that although the final PRD function shows a noticeable difference in the standard deviation (0.209 from step-by-step calculation vs. 0.268 from time averaging), the mean values are very close (1.68 *nm* vs 1.67 *nm*). The corresponding ECSA decay rates are almost identical for potentials higher than 0.85 V and show a relative error of less than 10% from 0.7 to 0.85 V. We conclude that time-averaging the PRD function gives a fairly good approximation of the actual evolution of the PRD function, and the corresponding ECSA decay rate is close enough to deliver similar results for the decayed ECSA. Thus, in the long-term simulations performed in this paper, the new PRD function is calculated using the time-averaged approach over each time interval. The corresponding ECSA decay rates for different potentials are calculated, and then used to get the total ECSA decay for each time interval. This procedure is repeated until the ECSA drops below the threshold.

After calculating the ECSA decay rate under constant potential hold, the effects of transient power demand, startup/shutdown cycles, and high power load are introduced into the

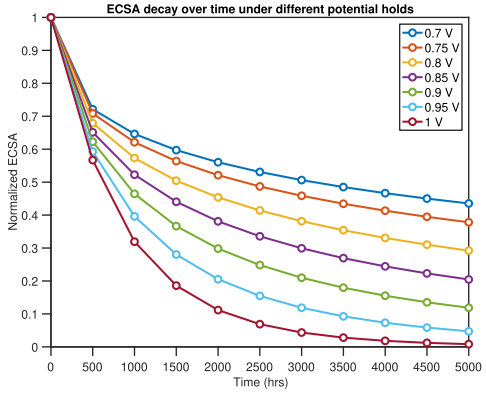

(a) Decay of normalized ECSA under different potential holds over 5000 hours.

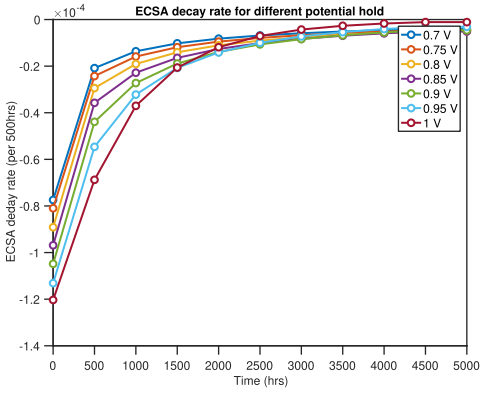

(b) ECSA decay rate over time under different potentials.

Fig. 2 – Normalized ECSA decay rate under different potentials.

fuel cell degradation model. The relative degradation effects of different conditions were studied in Ref. [35] which provides the following lifetime model for the fuel cell:

$$T_f = \frac{\Delta P}{k_p(P_1 n_1 + P_2 n_2 + P_3 t_1 + P_4 t_2)} \quad (7)$$

where ΔP is the maximum allowable performance decay (10%), and k_p is an accelerating factor that accounts for the difference in performance decay rate between the laboratory and real world drive cycles which is set to 1.72 in Ref. [35]. Parameters P_1, P_2, P_3 and P_4 are performance decay rates measured in the laboratory due to transient load changes, start-stop cycling, idling, and high power loading, respectively; n_1 is the number of transient load changes per hour of the drive cycle, n_2 is the number of start/stop cycles per hour of the drive cycle, and t_1 and t_2 are the fractions of the drive cycle spent in idling, and high power loading, respectively.

Our first objective here is to convert all the performance decay rates (P_1 to P_4) to their equivalent ECSA decay rates. Knowing the ECSA decay rate for each of the four degradation mechanisms will allow us to create a composite performance decay rate for our real-world driving schedule as opposed to the prescribed laboratory cycles employed by Ref. [35]. Of the four performance decay rates listed in Eq. (7), we will first address the performance decay rate P_3 [%/hour] due to idling which is associated with a high potential hold [35]; provides the value of P_3 under a potential hold of 0.9 V. P_3 can be directly correlated to an equivalent ECSA decay rate [1/hour] at 0.9 V using the ECSA decay model presented in Section Fuel cell degradation model based on ECSA loss. The method is further discussed and justified in Section Validation.

Before we continue, we would like to point out that the models employed in this study were gathered from a number of other studies cited above. The differences in experimental setups between the cited studies, such as flow field design and membrane electrode assembly (MEA) design, might affect the accuracy of the model especially considering that lifetime modeling relies heavily on empirical approaches. As mentioned above, we are linking the ECSA decay rate under open circuit voltage (OCV) hold (or high potential hold that is close to OCV) from Ref. [38] to the voltage drop rate measured under idling condition (close to zero current) from Ref. [35]. These two operating conditions are very similar, and they would be similar for any experimental setups under OCV hold or idling condition. Flow field design would not affect the ECSA decay rate under such conditions because the corresponding mass flux would be too small to be mass transport limited. The MEA design (membrane used, diffusion media thickness and composition, etc.) might affect the degradation of the stack. However, we had determined that the catalyst layer degradation is the major cause of performance decay based on our literature review in Section Degradation of the fuel cell and battery and thus we focused on catalyst layer degradation, i.e. ECSA decay, in our fuel cell degradation model. Hence, we would argue that the MEA design would not change the simulation results.

As a side note, by using the voltage drop rate under different operation conditions and the empirical acceleration factor k_p from Ref. [35], the end effects of other non-major degradation mechanisms can be considered to be already included in the resulting degradation in our model. Another concern might be that the relative voltage drop rates from Ref. [35] under different operation modes could be different for different fuel cell stacks. We are unable to confirm the fuel cell stack design from Ref. [35] and thus we assumed that the relative voltage drop rates would be similar across different stacks as a first attempt to justify the models used in this paper.

Next, we consider the performance decay rate P_4 under high power load which is denoted as the power when the cell voltage drops below 0.7 V as in Ref. [35]. As will be shown below in Section Effects of ECSA decay on the polarization curve, there is a roughly linear relationship between performance and remaining ECSA. Therefore, it is reasonable to assume that the ECSA decay under high power scales with the ECSA decay under idling according to the ratio P_4/P_3 which is obtained from Ref. [35]. Similarly, the ECSA decay rate due to transient power load change [1/ΔkW] is calculated by multiplying the ECSA decay rate at 0.9 V by the ratio P_1/P_3 which is also obtained from Ref. [35]. It should be noted that the power load fluctuation in Ref. [35] consisted of ramping the fuel cell power up to 60 kW and then dropping back down to idle power. Therefore, the value of P_1 [%/ΔkW] used here was obtained from its original value in the paper [%/load cycle] by dividing by 120 kW.

Finally, we examine the performance decay rate P_2 due to start/stop cycles which has some associated inconsistencies in the literature. According to Ref. [44], the fuel cell loses 23.91 μV per start/stop cycle. The corresponding performance loss from Ref. [35] is 0.00196 [%/cycle], which is equivalent to a decay of 13.72 [μV/cycle] using 0.7 V as the cell voltage under regular operating conditions. These two values are of similar order of magnitude. However, it has been shown that momentary purging (3s in Ref. [50]) after shutdown can reduce the residual high potential in the fuel cell and effectively eliminate the degradation associated with shutdown [37,53]. Further experiments with purging performed by Ref. [35] showed a dramatic decrease in the performance decay rate from 0.00196 to 0.000234 [%/cycle], which is equivalent to 0.16 [μV/cycle]. This is two orders of magnitude smaller than the 23.91 [μV/cycle] reported in Ref. [44]. Alternatively, it was suggested by Ref. [51] that the degradation cost of start/stop cycles can be represented by the time spent under high potential during start/stop cycling. Accordingly, we set the degradation due to start/stop cycles as equal to the ECSA decay for 3 s under a potential hold of 0.9 V.

At this point, we have converted the performance decay rates due to the four degradation mechanisms as measured under laboratory conditions to their equivalent ECSA decay rates. In the next section, we will use the ECSA decay rates to simulate the performance decay of our stack under real-world driving conditions.

Effect of ECSA decay on the polarization curve

The fuel cell potential is modeled by:

$$E = E_r + E_{act} + E_{ohm} + E_{mass} \quad (8)$$

where E_r is the standard-state reversible potential, E_{act} is the activation loss, E_{ohm} is the ohmic loss, and E_{mass} is the mass

transfer loss. The activation loss is calculated from the Tafel equation:

$$E_{act} = \frac{RT}{\alpha_t n_e F} ln\left(\frac{j}{j_o}\right) \tag{9}$$

where α is the charge transfer coefficient which is set to 0.5, n_e is the number of electrons transferred during the reaction which is equal to 2, F is the Faraday constant, and j is the current density. The exchange current density j_o is given by Ref. [52]:

$$j_o = j_o^{ref} A_{pt} \left(\frac{P_r}{P_r^{ref}}\right)^{\gamma} exp\left[-\frac{E_{red}}{RT}\left(1-\frac{T}{T_{ref}}\right)\right] \tag{10}$$

where j_o^{ref} is the reference exchange current density per unit catalyst surface area (A/cm^2), A_{pt} is the effective catalyst surface area ($[m^2/m^2]$), P is the reactant partial pressure, γ is the pressure coefficient, and E_{red} is the activation energy for O_2 reduction on Pt. T is the temperature and $T_{ref} = 298.15K$.

Under static operating conditions, all terms in Eq. (10) can be assumed to be constant and thus their absolute values are not relevant here. j_o is fitted to be 0.001164 A/cm^2 based on initial testing data of the fuel cell stack on our latest bus which is within the reported range from the literature [53]. Then it can be shown that j_o is proportional to A_{pt}:

$$j_o \propto A_{pt} \tag{11}$$

The activation loss due to ECSA decay can be described as:

$$E_{act} = -\frac{RT}{\alpha n_e F} ln\left(\frac{jA_{pt}^0}{j_o A_{pt}^t}\right) = -\frac{RT}{\alpha n_e F}\left(ln\left(\frac{j}{j_o}\right) - ln(\alpha_{pt})\right) \tag{12}$$

where A_{pt}^0 and A_{pt}^t denote the A_{pt} at the initial and current time. Parameter A_{pt}^0 is set to be 71 m^2/m^2 from Ref. [27]. Note that the ECSA decay term results in a constant increase in the activation loss across the entire current range. We denote the remaining ECSA as $\alpha_{pt} = A_{pt}^t/A_{pt}^0$.

The mass transfer loss E_{mass} can be modeled as:

$$E_{mass} = \beta_e \frac{RT}{4F} ln\left(1-\frac{j}{j_{lim}}\right) \tag{13}$$

where β_e is an empirical parameter that accounts for the difference between the ideal and real fuel cell conditions where oxygen transport could be hindered by water accumulation. Parameter β_e is set to 10 and the resulting coefficient for the exponential term $\beta_e RT/4F$ is 0.076 V which is close to the typical value of 0.1 V in PEMFC modeling [54]. Variable j_{lim} is the limiting current density, which is related to the oxygen concentration in the flow field channel c_o and the total oxygen transfer resistance $R_{O_2,total}$ by:

$$j_{lim} = 4F\frac{c_o}{R_{O_2,total}} \tag{14}$$

where $R_{O_2,total}$ is defined by:

$$R_{O_2,total} = R_{O_2,CL} + R_{O_2,DM} = \frac{\Delta c}{N_o} = 4F\frac{c_o - c_i}{j} \tag{15}$$

where $R_{O_2,CL}$ and $R_{O_2,DM}$ are the transfer resistance of the catalyst layer, and diffusion media including both the micro porous layer and gas diffusion layer, respectively. Here c_i is the local molar concentration of oxygen and N_o is the oxygen flux.

The oxygen transfer resistance of the catalyst layer is directly influenced by the ECSA and [27] gives an expression based on experimental data:

$$R_{O_2,CL} = \frac{C_1}{A_{pt}^t} + C_2 \tag{16}$$

where C_1 is set to 1700 s/m and C_2 is set to 5 s/m to reflect the effect of ECSA decay on transfer resistance [27].

The limiting current density after aging is given by:

$$j_{lim} = \left(\frac{\frac{C_1}{A_{pt}^0} + C_2 + R_{O_2,DM}}{\frac{C_1}{\alpha_{pt}A_{pt}^0} + C_2 + R_{O_2,DM}}\right) j_{lim}^0 \tag{17}$$

where j_{lim}^0 is the limiting current in the initial polarization curve and is set to 2.2 A/cm^2 based on [27]. Parameter $R_{O_2,DM}$ is set to 210 s/m to get similar polarization curves before and after aging, as shown in Ref. [27]. Setting $R_{O_2,DM}$ to 210 s/m is a reasonable assumption based on the relative magnitudes of $R_{O_2,DM}$ and $R_{O_2,CL}$ as measured in Ref. [28] which shows that $R_{O_2,CL}$ (the pressure independent term R_{other} in Ref. [28]) accounts for 15% of the total resistance compared to 12% used here (29/(29 + 210)). It should be noted that the relative magnitude of $R_{O_2,CL}$ will increase over time due to the effect of the ECSA loss term A_{pt}^t in Eq. (16).

The ohmic resistance R_{ohm} also increases with time [55]. The degradation rate r per cell is set to 2.508×10^{-7} Ω/h which is an empirical parameter used in Ref. [33]. It is appropriate to apply the ohmic increase rate in place of the area specific resistance because the fuel cell stack studied in that paper and the one used in our bus have almost identical active areas (280 cm^2 vs. 285 cm^2). Finally, the voltage of the fuel cell can be expressed as:

$$\begin{aligned} V = & E_{ocv} - \frac{RT}{\alpha n_e F}\left(ln\left(\frac{j}{j_o}\right) - ln(\alpha_{pt})\right) \\ & + \beta\frac{RT}{4F} ln\left(1 - \left(\frac{\frac{C_1}{\alpha_{pt}A_{pt}^0} + C_2 + R_{O_2,DM}}{\frac{C_1}{A_{pt}^0} + C_2 + R_{O_2,DM}}\right)\frac{j}{j_{lim}^0}\right) - j(R_{ohm} + rt) \end{aligned} \tag{18}$$

The open circuit voltage E_{ocv} is equal to the reversible voltage minus the activation loss associated with the leaking current j_{leak}. Therefore, j_{leak} does not appear explicitly in Eq. (18). The initial (beginning-of-life) polarization curve fitted to the data collected from our fuel cell bus is shown in Fig. 3 (the curve with ECSA = 1) where j_o and R_{ohm} are fit to be 0.001164 A/cm^2 and 0.1283 $\backslash ohmcm^2$. Note, however, that the vehicle configuration used in this study is scaled up from the UD fuel cell bus to match the performance obtained during DOEs recent American Fuel Cell Bus (AFCB) projects carried out by Sunline Transit Agency and MBTA [56] which employed a FCvelocity-HD6, 150 kW fuel cell stack (Ballard) and a Nanophosphate Li-ion, 200 kW, 11 kWh battery pack.

The simulated polarization curves for diminishing ECSAs are shown in Fig. 3a. Also shown is the peak net power of the fuel cell stack which drops steadily with diminishing ECSA.

Our criterion for end-of-life (EOL) is similar to the one used in Ref. [35], which corresponds to a 10% voltage drop for a constant current. The current used in Ref. [35] is the current density at a beginning-of-life voltage of 0.7 V. We employ a current density of 0.5 A/cm^2 which corresponds to

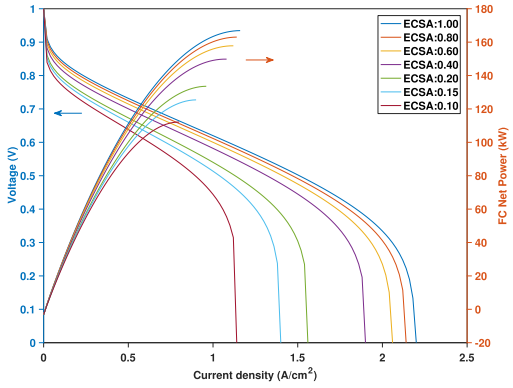

(a) Effect of diminishing ECSA on the polarization curve and fuel cell net power over time.

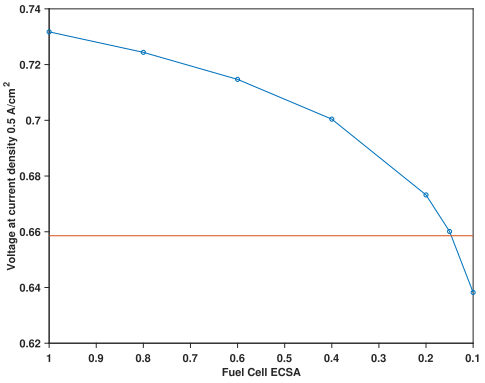

(b) Effect of diminishing ECSA on the voltage drop at 0.5 A/cm^2.

Fig. 3 – Effect of diminishing ECSA on (a) polarization curves, and (b) the resulting voltage drop at 0.5 A/cm^2 where 10% voltage drop corresponds to EOL at about 0.66 V and 15% remaining ECSA.

the most frequently used power range. The voltage drop is then calculated for diminishing ECSA. As shown in Fig. 3b, the voltage drop is initially linear and then accelerates after the ECSA falls below 40%. A 10% performance drop corresponds to about 15% remaining ECSA which is used to mark the EOL of the fuel cell stack in the lifetime simulations conducted in this work.

Validation

We now compare the voltage drop rate calculated from the ECSA decay model to the reported experimental data under idling conditions from Refs. [35,36] to provide validation of our approach to model degradation of the fuel cell stack. The data reported in Refs. [35,36] was collected under a controlled laboratory environment where the idling condition is defined as operating the fuel cell at 10 mA/cm^2 and 0.9 V. Thus, in our analysis the ECSA decay rate at 0.9 V is used to calculate the corresponding voltage drop rate based on the polarization curve. The results are shown in Fig. 4. The two reported voltage drop rates from lab test data, averaged over a period of 200 h, are 8.662 $\mu V/h$ [36] (grey line), and 11.55 $\mu V/h$ [35] (pink line). Our voltage drop rate calculated from the ECSA decay rate under a potential hold of 0.9 V is plotted against time (red curve), and the corresponding cumulative average voltage drop rate (blue curve) is also shown in Fig. 4. It should be noted that since the ECSA decay rates will decrease over time, it is more reasonable to compare the average resulting voltage drop rate throughout the lifetime of the stack, which is exactly how the voltage drop rate was used in the model from Refs. [35,36]. The reported real world lifetime from Ref. [36] is around 1100 h. As only the lab test results are compared here, the real world lifetime is scaled up by the accelerating factor k_p defined in Eq. (7) to obtain a lab lifetime of 1892 h. The cumulative average voltage drop rate in Fig. 4 is around 10 $\mu V/h$ at 1892 h which falls right between the reported average values. Therefore, we conclude that it is reasonable to link the experimental voltage decay rate from Refs. [35,36] to the ECSA decay rate used in our model as described in Section ECSA degradation model to model the ECSA decay and fuel cell degradation under various driving conditions.

Lithium-ion battery degradation model based on discharged Ah throughput

Degradation of the Li-ion battery is simulated using the model from Ref. [57], which describes the instantaneous battery capacity loss rate as a function of current. The model is based on a semi-empirical experimentally-validated capacity loss model [46]:

$$\Delta Q_b = M(c) exp\left(\frac{-E_a(c)}{RT}\right) A(c)^z \tag{19}$$

where ΔQ_b is the percentage capacity loss, c is the charging/discharging rate (C-rate) and $M(c)$ is the pre-exponential factor

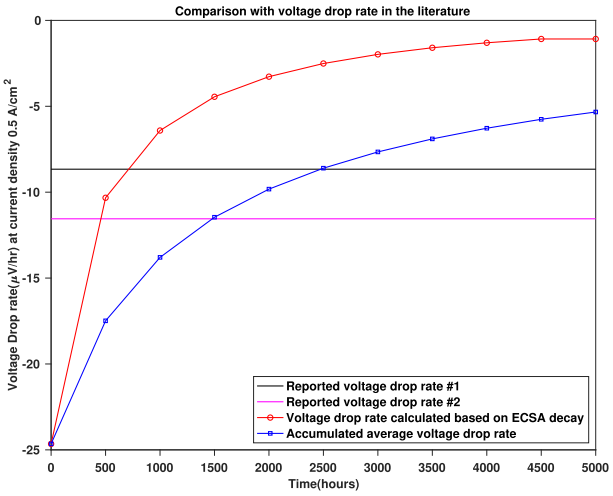

Fig. 4 – Comparison of the voltage drop rate calculated from the ECSA decay rate with the experimental results from Refs. [35,36] under idling conditions. The reported voltage drop rates are 8.662 $\mu V/h$[36] (grey line) and 11.55 $\mu V/h$[35] (pink line). The calculated voltage drop rate based on the ECSA decay rate under 0.9 V potential hold and its average values throughout the lifetime of the fuel cell stack (around 1892 h) fall within the reported range. (For interpretation of the references to colour in this figure legend, the reader is referred to the Web version of this article.)

as a function of the C-rate. Variable A is the discharged Ah throughput depending on C-rate. The activation energy E_a and the power-law factor z are given by:

$$E_a(c) = 31700 - 370.3c, \qquad z = 0.55 \tag{20}$$

Since a capacity loss of 20% is often considered the EOL for a battery in automotive applications [57], we assign $\Delta Q_b = 20\%$ in Eq. (19). Then the total discharged Ah throughput A_{total} and corresponding number of cycles N until EOL can be calculated as follows:

$$A_{total}(c, T_c) = \left[\frac{20}{M(c)exp\left(\frac{-E_a(c)}{RT}\right)}\right]^{\frac{1}{z}} \tag{21}$$

$$N(c, T_c) = \frac{A_{total}(c, T_c)}{C_{bat}} \tag{22}$$

where C_{bat} is the nominal capacity of the battery in Ah. The remaining battery capacity can be calculated as:

$$Q(t) = Q(t_0) - \frac{\int_{t_0}^{t} \left|I(\tau)\right| d\tau}{2 \times 3600 N(c, T_c) C_{bat}} \tag{23}$$

and the battery capacity decay rate is derived by differentiating equation Eq. (23):

$$\dot{Q}(t) = -\frac{|I(t)|}{2N(c, T_c) C_{bat}} \tag{24}$$

Solving Eq. (24) gives the battery state-of-health (SoH) decay rate as shown in Fig. 5.

Formulation of optimal control problem

The optimization objective is to minimize the overall lifetime cost of the hybrid system by minimizing the fuel consumption and maximizing the lifetime of the fuel cell and battery. Hence, the objective function is defined as:

$$minJ = \int_0^T \left(c_{h_2}\dot{m}_{h_2} + \alpha\left(c_{fc}\dot{A}_{Pt} + c_{fcp}\dot{P}_{fc} + c_{cyl}C + c_{fch}\right) + \beta c_{bat}\dot{B}_{soh}\right) dt \tag{25}$$

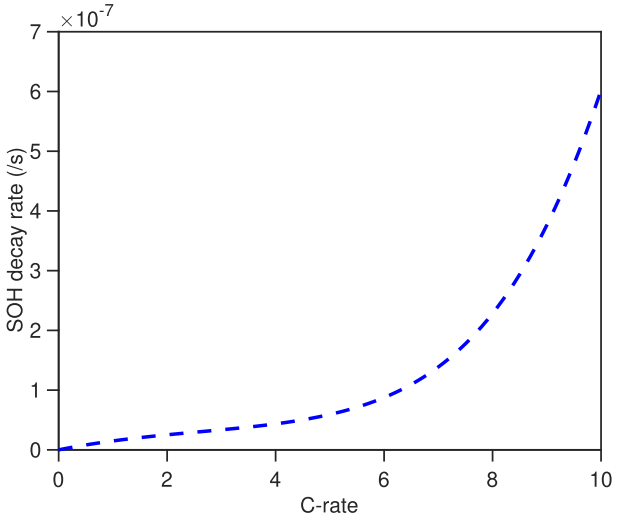

Fig. 5 – Battery SoH decay rate as a function of C-rate.

$$state: x_k = \left(SoC_k, P_{fc}^{k-1}\right)$$

$$control: u(k) = P_{fc}^{k} \tag{26}$$

$$subject\ to: P_{fc}^{k} \in (P_{min}, P_{max}) \tag{27}$$

$$SoC_k \in (SoC_{min}, SoC_{max}) \tag{28}$$

The state variables are the current battery state-of-charge SoC_k, and the fuel cell power at the previous timestep P_{fc}^{k-1} which is used to constrain the fuel cell power ramp rate. The battery SoC is also constrained between predetermined limits. The control variable P_{fc}^{k} is directly determined by the optimal state trajectory in this formulation.

The hydrogen price c_{h_2} is set to $ 2/kg based on the DOE 2020 target for the levelized cost of hydrogen using centralized water electrolysis [58], and $\dot{m}_{h_2}$ is the hydrogen consumption rate. The fuel cell degradation cost consists of four parts whose values are determined from Eq. (7). The cost due to ECSA decay c_{fc} is determined by assuming an 85% ECSA loss at the EOL of the fuel cell stack whose replacement cost is based on the DOE 2020 target of $\$40/kW_{net}$ [59]. It is then multiplied with the ECSA decay rate $\dot{A}_{Pt}$ to get the decay cost under high constant potential. Costs due to the other three degradation mechanisms are calculated as discussed in Section ECSA degradation model. The cost due to the transient power load change c_{fcp} is multiplied by the fuel cell power fluctuation $\dot{P}_{fc}$. The cost due to startup/shutdown cycles c_{cyl} is multiplied by the number of cycles C. The cost under high fuel cell power load c_{fch} is a constant. The battery decay cost is defined as the SoH decay rate $\dot{B}_{soh}$ which is a function of C-rate, multiplied by the capital cost to replace the battery c_{bat}.

Weights α and β are cost factors to balance the relative weight of the degradation cost of the fuel cell and the battery. The relative magnitude of the degradation cost of the fuel cell and the battery is determined by the values (between 0 and 1) assigned to α and β as demonstrated in Section Effect of including degradation on power management. The cost of the Li-ion battery is determined by assuming a total SoH loss at the EOL of the battery whose replacement cost is based on the DOE 2022 target of $\$125/kWh$ [60].

The optimization problem is solved using a deterministic dynamic programming algorithm (DP), whose detailed theory and implementation can be found in Ref. [61].

Results and discussions

Data collected from a campus drive cycle at the University of Delaware are used for all the simulations presented in this section. This drive cycle is representative of a typical urban transit loop. It consists of frequent stops and starts and low to medium average speeds on mostly flat roads. The initial and final battery SoCs are set to 0.7. The velocity profile and corresponding measured power demand are shown in Fig. 6.

In the following sections, we first investigate the effect of varying the relative weight attached to fuel cell degradation on the resulting power management strategies during the initial portion (first 100 h) of system lifetime. Next, we

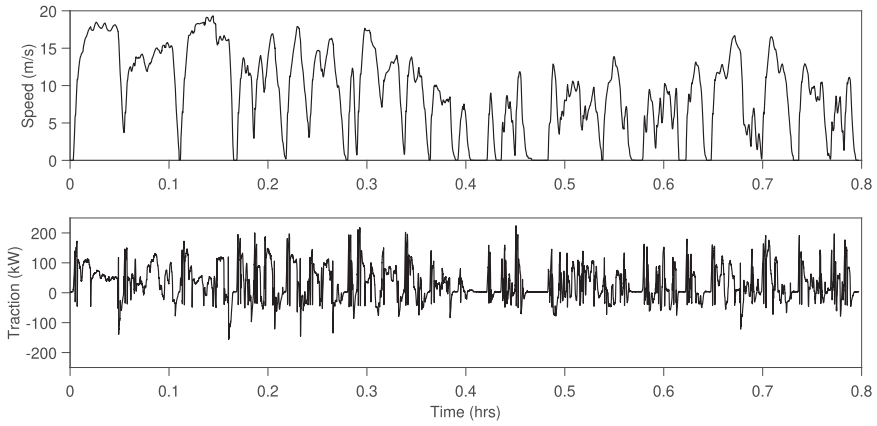

Fig. 6 – Drive cycle data collected from a campus drive cycle at the University of Delaware used for all simulations.

examine the cost effects of fuel cell and battery degradation over the entire lifetime of the system. Finally, we present how the optimal power management strategy might shift over the lifetime of the vehicle due a change in the systems performance characteristics.

Effect of including degradation on power management

Here, we focus only on the effect of the fuel cell degradation cost factor α (see Eq. (25)). The cost factor of the battery β is set to a constant value of 1.0 considering its relatively low cost compared to the fuel cell stack. Accordingly, α is set to 0.01, 0.1, and 1.0, and the resulting optimal power management strategies for the first 100 h of system lifetime are shown in Fig. 7. We consider $\alpha = 0.01$ as the baseline case since it assigns a very small cost factor to the fuel cell degradation, which replicates a power management strategy that ignores the cost of fuel cell degradation. We set $\alpha = 0.01$ rather than 0 for the baseline case as $\alpha = 0$ results in an untenable power profile wherein the fuel cell experiences excessive transient power fluctuations and startup/shutdown cycles which would greatly shorten its lifetime. Setting α to 0.01 can effectively eliminate such unrealistic operating scenarios. On the other hand, setting $\alpha = 1.0$ corresponds to a power management strategy which tries to minimize the total degradation cost of the fuel cell system over its lifetime. An intermediate value of $\alpha = 0.1$ was also selected to fully examine the cost effect of fuel cell degradation.

Figure Fig. 7 shows that the resulting fuel cell power profile for $\alpha = 0.01$ (blue curve) is typical of a fuel cell-dominant (load-following fuel cell) vehicle with frequent power fluctuations and start/stop cycles. This type of load-following power management strategy is typically employed in the literature to study the durability of fuel cell-dominated vehicles. Increasing α to 0.1 (red curve) effectively eliminates the start/stop cycles and greatly suppresses the fuel cell power fluctuations. Now, the fuel cell turns on at the beginning of the drive cycle and remains on till the very end. Further increase of α to 1.0 completely eliminates the power fluctuations which means that the optimal control for this case is for the fuel cell

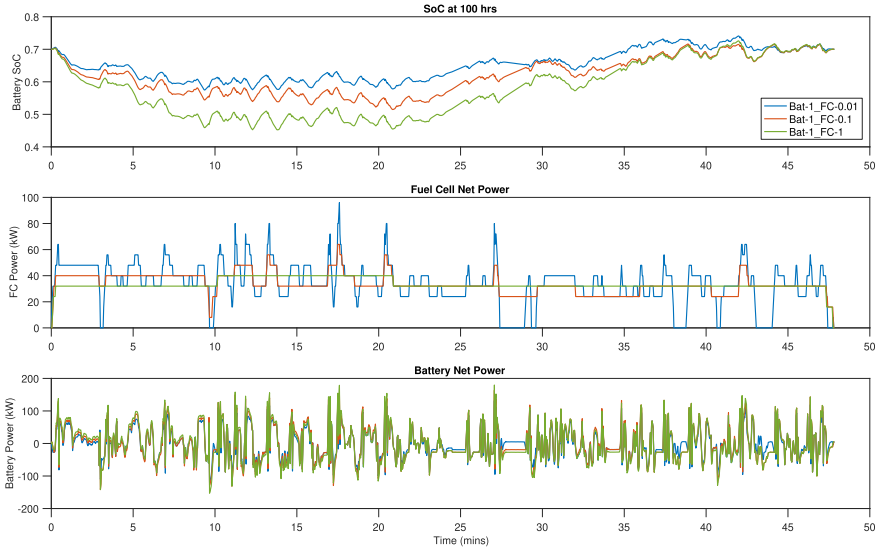

Fig. 7 – Optimal fuel cell power profile for the first 100 h for fuel cell cost factors of α = 0.01, 0.1 and 1.0 with battery cost factor β = 1.0.

to operate around its peak fuel efficiency all the time without ever changing power or shutting down.

Effect of including degradation on system lifetime

The results of the previous section, which pertained only to the initial portion (first 100 h) of system lifetime, are now extended for the entire lifetime (5000 h). The optimal fuel cell power profile is calculated at various time points (as shown with the markers in Fig. 8a) throughout the lifetime of the fuel cell stack. The time points are spaced more closely together during the initial phase when degradation is rapid (every 100 h apart for the first 400 h) and are then gradually spaced further apart (every 200 h up to 1000 h, every 500 h up to 3000 h, and finally every 1000 h after 3000 h). The ECSA and battery decay are calculated after each DP simulation and then applied to the corresponding periods between time points. A new polarization curve is calculated based on the remaining ECSA after each DP simulation which is used to update the performance of the degraded fuel cell stack in the next DP simulation. This approach has been verified to accurately represent the actual ECSA decay while also reducing computation time.

The simulation results for a drive cycle lasting up to 5000 h are shown in Fig. 8. As expected, the fuel cell lifetime increases dramatically with increasing α. The baseline power management strategy which ignores fuel cell degradation ($\alpha = 0.01$) shows the fastest ECSA decay. The ECSA drops below the failure threshold of 15% in 1842 h, which is very close to the predicted lifetime of 1900 h for the #2 fuel cell bus in Ref. [36] which also operated under a rough fuel cell cycle similar to the fuel cell power profile shown in Fig. 7 (the $\alpha = 0.01$ case). This provides further validation of the effectiveness of the ECSA decay-based performance degradation model developed in this paper.

Increasing α to 0.1 extends the lifetime by 70% over the baseline case to 3124 h. Further increase of α to 1.0 achieves a lifetime of 4086 h which is more than double the baseline case and close to the DOE target of 5000 h. Interestingly, the fuel consumption is very similar across the three different cases as shown in Fig. 8c. However, it is noticeable that the fuel consumption rate starts to increase for the baseline case after 1500 h due to the extremely low ECSA which corresponds to low fuel cell performance. The battery SoH decay shown in Fig. 8b is mostly linear for each case, but the decay rates differ substantially. The SoH decay rates for the first 2000 h are -0.23, -0.30 and -0.42 for $\alpha = 0.01$, 0.1 and 1.0, respectively. The SoH decay is linearly extrapolated to calculate the battery degradation cost at 5000 h. The baseline case would result in a much higher final SoH close to 43%, compared to $\alpha = 1$ which almost results in a failed battery at 5000 h.

Finally, the average running cost for each case is shown in Fig. 8d. The baseline power management cost is $7.96 per hour of vehicle operation; increasing α to 0.1 and 1.0 results in a cost reduction of 19% and 25%, respectively. It is worth noting that the fuel costs are similar for each case, and the battery cost is relatively small compared to the cost of the fuel and stack. The major cost difference arises from the degradation cost of the fuel cell stack.

Changes in the optimal power management strategy over system lifetime

It is reasonable to expect that the optimal power management strategy should shift as the systems performance

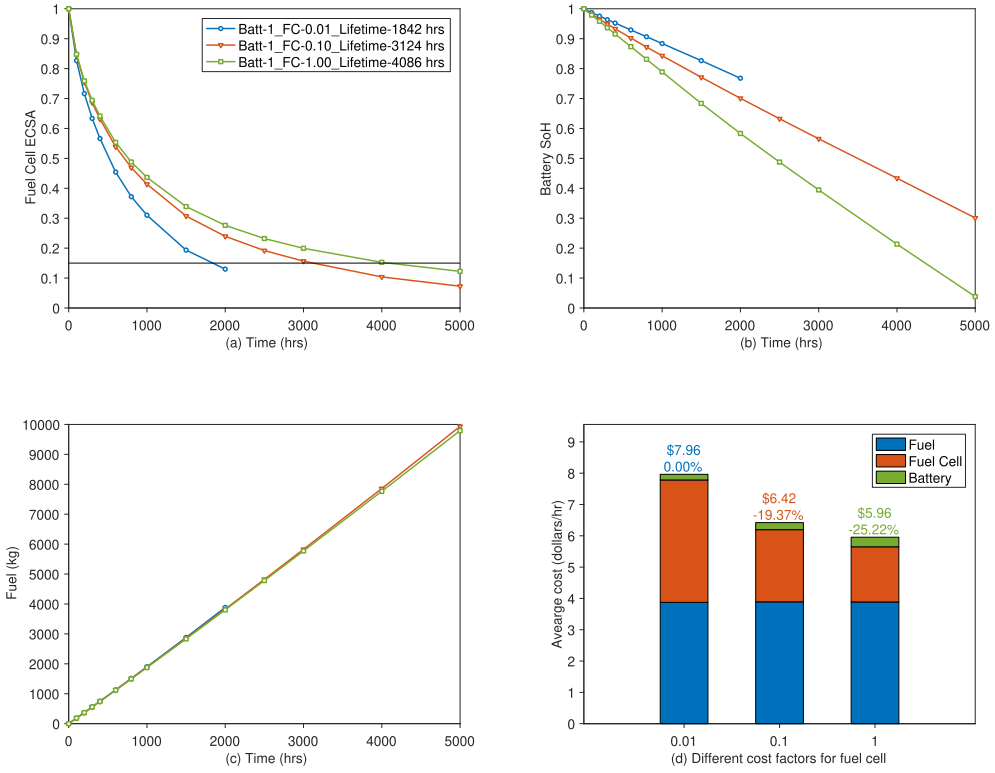

Fig. 8 – Comparison of (a) fuel cell and (b) battery degradation, (c) fuel consumption, and (d) total cost calculated at EOL.

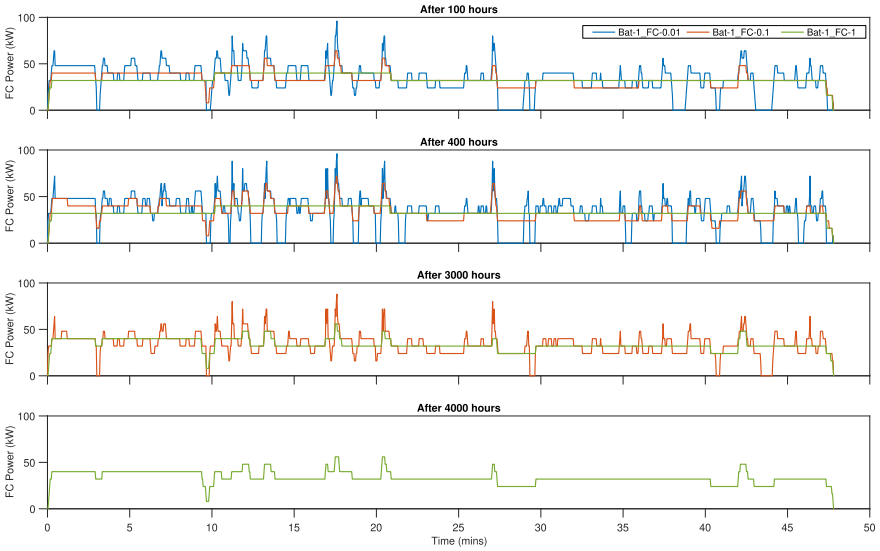

Fig. 9 – Optimal fuel cell power profile after 100, 400, 3000 and 4000 h over the lifetime of the fuel cell stack with different cost factors. Note that the fuel cell stack with $\alpha = 0.01$ has reached its EOL at 1842 h, and hence the FC power profile is not shown for 3000 and 4000 h. Similarly, the stack fails around 3000 h for $\alpha = 0.1$.

characteristics change due to degradation over its lifetime. The resulting optimal power profiles for the fuel cell stack at various times are shown in Fig. 9. From Fig. 8a it is apparent that the ECSA decay rate becomes less steep over time and therefore, the power management system would be expected to apply greater stress on the fuel cell stack at later times. Therefore, after 400 h, the baseline case (blue curve) shows a more aggressive fuel cell load profile with more frequent load fluctuations and start/stop cycles compared to the 100 h profile. After 3000 h, the fuel cell for the $\alpha = 0.1$ case (red curve) is close to its EOL. The decreasing ECSA decay rate results in a fuel cell load profile with higher power fluctuations and more start/stop cycles that is in fact quite similar to the $\alpha = 0.01$ case at the beginning of life (100 h). After 4000 h, the fuel cell for the $\alpha = 1$ case (green curve) is also close to its EOL and begins to exhibit greater power fluctuations, although still without any shutdowns.

This clearly shows that as the fuel cell stack ages and the ECSA decay rate declines, the cost factor attached to the fuel cell degradation term should decrease, and the controller should start to favor fuel consumption and battery SoH rather than fuel cell degradation. Thus, the optimal control strategy would be to operate the fuel cell at a more or less constant power level at the beginning of the life, and gradually shift to a more load-following power management strategy later in its lifetime as required for performance.

Conclusions

An electrochemical surface area (ECSA) degradation model and an empirical lifetime model of the fuel cell stack are combined to model the decay of ECSA over the lifetime of the fuel cell stack in a fuel cell/battery hybrid transit vehicle. The predicted lifetime of the fuel cell stack for the baseline case (which ignores stack degradation) shows good agreement with the lifetime reported in the literature. Next, models for the fuel cell degradation and the battery capacity decay are added to the power management formulation of the hybrid vehicle to study their effects on the optimal power management strategy and system lifetime. It is shown that assigning different cost factors to the fuel cell degradation results in dramatically different power load profiles for the fuel cell stack, which greatly affects lifetime. A smaller weight factor produces a more aggressive load-following profile for the fuel cell stack resembling a power load controller, whereas a larger weight factor results in a smoother power load profile.

The baseline case (cost factor = 0.01) results in a load profile similar to typical transient load profiles and yields a short lifespan under 2000 h. On the other hand, increasing the cost factor to 1.0 can extend the lifetime to over 4000 h, which approaches the DOE target for fuel cell lifetime. It is also shown that the battery SoH decay rate varies with different fuel cell cost factors despite its relatively small cost compared to the fuel and the fuel cell stack. The ECSA decay rate becomes less steep as the ECSA diminishes over the lifetime of the fuel cell and therefore, the control strategy can be modified over time to apply a more aggressive load on the fuel cell stack.

The conclusions drawn from this research are based on DOE's target costs and the current degradation characteristics of the fuel cell and battery system. Future changes in the cost or degradation rate of system components might yield different results. This model can be easily adjusted to simulate new improved systems by measuring the initial ECSA and Pt dissolution rate under constant potential hold, which could yield different rates for ECSA decay and performance drop, as well as system lifetime. It should also be noted that the ECSA decay shown in all results is the normalized ECSA. Increasing the initial Pt loading and thus the actual ECSA can further prolong stack life which might actually reduce the average cost over system lifetime, despite higher initial capital cost. In

an ongoing effort, we are conducting a parameter sizing study to optimize the hybrid platform that provides the least overall lifetime cost as well as the potential of real-time implementation using the models studied in this paper.

Acknowledgments

This work was conducted under the University of Delaware's Fuel Cell Bus Program to research, build, and demonstrate fuel cell powered hybrid vehicles for transit applications. This program is funded by the Federal Transit Administration and the Mid-Atlantic Transportation Sustainability Center University Transportation Center at the Center for Fuel Cells and Batteries at the University of Delaware.

Nomenclature

α, β	Cost factors of degradation terms
α_t	Charge transfer coefficient
$\overline{V}_{Pt}$	Molar volume of Pt, $[m^3/mol]$
β_e	Empirical parameter in mass transfer loss
β_t	Transfer coefficient
ΔP	Maximum allowable performance decay
ΔQ_b	The percentage capacity loss of battery
γ	Pressure coefficient
γ_{Pt}	Surface tension, $[N/m]$
$\dot{B}_{soh}$	Battery SoH decay rate, $[1/s]$
$\dot{m}_{h_2}$	hydrogen consumption rate, $[g/s]$
T	Dimensionless time
θ_{PtO}	PtO coverage in percentage
ξ	Dimensionless radius
A	Discharged Ah throughput, $[Ah]$
A_{pt}	Effective catalyst surface area
C	The number of on/off cycles
c	Charging/discharging rate (C-rate)
c_i	Local molar concentration of oxygen, $[mol/m^3]$
C_{bat}	The nominal capacity of the battery, $[Ah]$
c_{bat}	Battery replacement cost
c_{fc}, c_{fcp}, c_{cyl}, c_{fch}	Fuel cell degradation costs under different operation modes
c_{h_2}	Hydrogen price
E_a	Activation energy, $[J/mol]$
E_r	Standard-state reversible potential, $[V]$
E_{act}	Activation loss, $[V]$
E_{mass}	Mass transfer loss, $[V]$
E_{ocv}	Open circuit voltage, $[V]$
E_{ohm}	Ohmic loss, $[V]$
E_{red}	Activation energy for O_2 reduction on Pt, $[J/mol]$
F	Faraday constant, $[C/mol]$
j	Current density, $[A/cm^2]$
j_o^{ref}	Reference exchange current density, $[A/cm^2]$
j_{lim}	Limiting current density, $[A/cm^2]$
k_p	Accelerating factor for real world drive cycles
k_{Pt}^{∞}	Effective bulk rate constant for Pt–O dissolution, $[mol/m^2s]$
$M(c)$	Empirical pre-exponential factor
n_1	Number of transient load changes per hour
n_2	Number of start/stop cycles per hour
n_e	Number of electrons transferred during the reaction
N_o	Oxygen flux, $[mol/m^2s]$
P	Reactant partial pressure, $[Pa]$
P_i	Fuel cell performance decay rate under different operation modes
P_{fc}	The change rate of fuel cell power, $[kW/s]$
$Q(t)$	The remaining battery capacity
$R_{O_2,CL}$	Transfer resistance of the catalyst layer, $[s/m]$
$R_{O_2,DM}$	Transfer resistance of the diffusion media, $[s/m]$
$R_{O_2,total}$	Total transfer resistance, $[s/m]$
T	Temperature, $[K]$
t_1	Fraction of the drive cycle spent in idling
t_2	Fraction of the drive cycle spent under high power
w	Interaction energy, $[kJ/mol]$

REFERENCES

[1] Scrosati B, Garche J. Lithium batteries: status, prospects and future. J Power Sources 2010;195(9):2419–30. https://doi.org/10.1016/j.jpowsour.2009.11.048. http://www.sciencedirect.com/science/article/pii/S0378775309020564.

[2] Lu L, Han X, Li J, Hua J, Ouyang M. A review on the key issues for lithium-ion battery management in electric vehicles. J Power Sources 2013;226:272–88. https://doi.org/10.1016/j.jpowsour.2012.10.060. http://www.sciencedirect.com/science/article/pii/S0378775312016163.

[3] Thomas C. Fuel cell and battery electric vehicles compared. Int J Hydrog Energy 2009;34(15):6005–20. https://doi.org/10.1016/j.ijhydene.2009.06.003. http://www.sciencedirect.com/science/article/pii/S0360319909008696.

[4] Wikipedia, Toyota Mirai — wikipedia, the free encyclopedia. 2016 [Online; accessed 1-July-2016], https://en.wikipedia.org/w/index.php?title=Toyota_Mirai&oldid=726813544.

[5] Bubna P, Brunner D, Gangloff Jr JJ, Advani SG, Prasad AK. Analysis, operation and maintenance of a fuel cell/battery series-hybrid bus for urban transit applications. J Power Sources 2010;195(12):3939–49. https://doi.org/10.1016/j.jpowsour.2009.12.080. http://www.sciencedirect.com/science/article/pii/S0378775309023428.

[6] Martinez CM, Hu X, Cao D, Velenis E, Gao B, Wellers M. Energy management in plug-in hybrid electric vehicles: recent progress and a connected vehicles perspective. IEEE Transactions on Vehicular Technology PP 2016;(99). https://doi.org/10.1109/TVT.2016.2582721. 1–1.

[7] Sulaiman N, Hannan M, Mohamed A, Majlan E, Daud WW. A review on energy management system for fuel cell hybrid electric vehicle: issues and challenges. Renew Sustain Energy Rev 2015;52:802–14. https://doi.org/10.1016/j.rser.2015.07.132. http://www.sciencedirect.com/science/article/pii/S1364032115007790.

[8] Bubna P, Brunner D, Advani SG, Prasad AK. Prediction-based optimal power management in a fuel cell/battery plug-in hybrid vehicle. J Power Sources 2010;195(19):6699–708. https://doi.org/10.1016/j.jpowsour.2010.04.008. http://www.sciencedirect.com/science/article/pii/S0378775310005896.

[9] Wu J, Yuan XZ, Martin JJ, Wang H, Zhang J, Shen J, Wu S, Merida W. A review of PEM fuel cell durability: degradation mechanisms and mitigation strategies. J Power Sources 2008;184(1):104–19. https://doi.org/10.1016/j.jpowsour.2008.06.006. http://www.sciencedirect.com/science/article/pii/S0378775308011968.

[10] Borup R, Meyers J, Pivovar B, Kim YS, Mukundan R, Garland N, Myers D, Wilson M, Garzon F, Wood D, Zelenay P, More K, Stroh K, Zawodzinski T, Boncella J, McGrath JE,

Inaba M, Miyatake K, Hori M, Ota K, Ogumi Z, Miyata S, Nishikata A, Siroma Z, Uchimoto Y, Yasuda K, Kimijima K-i, Iwashita N. Scientific aspects of polymer electrolyte fuel cell durability and degradation. Chem Rev 2007;107(10):3904–51. https://doi.org/10.1021/cr050182l. https://doi.org/10.1021/cr050182l.

[11] Jahnke T, Futter G, Latz A, Malkow T, Papakonstantinou G, Tsotridis G, Schott P, Grard M, Quinaud M, Quiroga M, Franco A, Malek K, Calle-Vallejo F, de Morais RF, Kerber T, Sautet P, Loffreda D, Strahl S, Serra M, Polverino P, Pianese C, Mayur M, Bessler W, Kompis C. Performance and degradation of proton exchange membrane fuel cells: state of the art in modeling from atomistic to system scale. J Power Sources 2016;304:207–33. https://doi.org/10.1016/j.jpowsour.2015.11.041. http://www.sciencedirect.com/science/article/pii/S0378775315305395.

[12] Wang Y, Chen KS, Mishler J, Cho SC, Adroher XC. A review of polymer electrolyte membrane fuel cells: technology, applications, and needs on fundamental research. Appl Energy 2011;88(4):981–1007. https://doi.org/10.1016/j.apenergy.2010.09.030. http://www.sciencedirect.com/science/article/pii/S0306261910003958.

[13] Shao Y, Yin G, Gao Y. Understanding and approaches for the durability issues of pt-based catalysts for PEM fuel cell. J Power Sources 2007;171(2):558–66. https://doi.org/10.1016/j.jpowsour.2007.07.004. http://www.sciencedirect.com/science/article/pii/S0378775307014814.

[14] Tabe Y, Nishino M, Takamatsu H, Chikahisa T. Effects of cathode catalyst layer structure and properties dominating polymer electrolyte fuel cell performance. J Electrochem Soc 2011;158(10):B1246–54. https://doi.org/10.1149/1.3624606. http://jes.ecsdl.org/content/158/10/B1246.abstract.

[15] Antolini E. Formation, microstructural characteristics and stability of carbon supported platinum catalysts for low temperature fuel cells. J Mater Sci 2003;38(14):2995–3005. https://doi.org/10.1023/A:1024771618027. https://doi.org/10.1023/A:1024771618027.

[16] Chen S, Gasteiger HA, Hayakawa K, Tada T, Shao-Horn Y. Platinum-alloy cathode catalyst degradation in proton exchange membrane fuel cells: nanometer-scale compositional and morphological changes. J Electrochem Soc 2010;157(1):A82–97. https://doi.org/10.1149/1.3258275. http://jes.ecsdl.org/content/157/1/A82.abstract.

[17] Stumper RRJ, Fuss F. In-situ diagnostic tools for fuel cell performance and degradation. ECS Trans 2009;25(1):1605–15. https://doi.org/10.1149/1.3210716.

[18] Ferreira PJ, la O GJ, Shao-Horn Y, Morgan D, Makharia R, Kocha S, Gasteiger HA. Instability of Pt/C electrocatalysts in proton exchange membrane fuel cells: a mechanistic investigation. J Electrochem Soc 2005;152(11):A2256–71. https://doi.org/10.1149/1.2050347. http://jes.ecsdl.org/content/152/11/A2256.abstract.

[19] Wang X, Li W, Chen Z, Waje M, Yan Y. Durability investigation of carbon nanotube as catalyst support for proton exchange membrane fuel cell. J Power Sources 2006;158(1):154–9. https://doi.org/10.1016/j.jpowsour.2005.09.039. http://www.sciencedirect.com/science/article/pii/S0378775305013522.

[20] Shao Y, Yin G, Gao Y, Shi P. Durability study of Pt/C and Pt/CNTs catalysts under simulated PEM fuel cell conditions. J Electrochem Soc 2006;153(6):A1093–7. https://doi.org/10.1149/1.2191147. http://jes.ecsdl.org/content/153/6/A1093.abstract.

[21] Wu J, Yuan X-Z, Martin JJ, Wang H, Yang D, Qiao J, Ma J. Proton exchange membrane fuel cell degradation under close to open-circuit conditions: Part i: in situ diagnosis. J Power Sources 2010;195(4):1171–6. https://doi.org/10.1016/j.jpowsour.2009.08.095. http://www.sciencedirect.com/science/article/pii/S0378775309015390.

[22] Yousfi-Steiner N, Mootguy P, Candusso D, Hissel D. A review on polymer electrolyte membrane fuel cell catalyst degradation and starvation issues: causes, consequences and diagnostic for mitigation. J Power Sources 2009;194(1):130–45. https://doi.org/10.1016/j.jpowsour.2009.03.060. xIth Polish Conference on Fast Ionic Conductors 2008, http://www.sciencedirect.com/science/article/pii/S0378775309005655.

[23] Taniguchi A, Akita T, Yasuda K, Miyazaki Y. Analysis of degradation in PEMFC caused by cell reversal during air starvation. Int J Hydrog Energy 2008;33(9):2323–9. https://doi.org/10.1016/j.ijhydene.2008.02.049. http://www.sciencedirect.com/science/article/pii/S0360319908002267.

[24] Taniguchi A, Akita T, Yasuda K, Miyazaki Y. Analysis of electrocatalyst degradation in PEMFC caused by cell reversal during fuel starvation. J Power Sources 2004;130(1):42–9. https://doi.org/10.1016/j.jpowsour.2003.12.035. http://www.sciencedirect.com/science/article/pii/S0378775304000096.

[25] Brightman E, Hinds G. In situ mapping of potential transients during start-up and shut-down of a polymer electrolyte membrane fuel cell. J Power Sources 2014;267:160–70. https://doi.org/10.1016/j.jpowsour.2014.05.040. http://www.sciencedirect.com/science/article/pii/S037877531400723X.

[26] Ohyagi S, Matsuda T, Iseki Y, Sasaki T, Kaito C. Effects of operating conditions on durability of polymer electrolyte membrane fuel cell pt cathode catalyst layer. J Power Sources 2011;196(8):3743–9. https://doi.org/10.1016/j.jpowsour.2010.12.068. http://www.sciencedirect.com/science/article/pii/S0378775310022767.

[27] Jomori S, Nonoyama N, Yoshida T. Analysis and modeling of PEMFC degradation: effect on oxygen transport. J Power Sources 2012;215:18–27. https://doi.org/10.1016/j.jpowsour.2012.04.069. http://www.sciencedirect.com/science/article/pii/S0378775312008038.

[28] Baker DR, Caulk DA, Neyerlin KC, Murphy MW. Measurement of oxygen transport resistance in PEM fuel cells by limiting current methods. J Electrochem Soc 2009;156(9):B991–1003. https://doi.org/10.1149/1.3152226. http://jes.ecsdl.org/content/156/9/B991.abstract.

[29] Nonoyama N, Okazaki S, Weber AZ, Ikogi Y, Yoshida T. Analysis of oxygen-transport diffusion resistance in proton-exchange-membrane fuel cells. J Electrochem Soc 2011;158(4):B416–23. https://doi.org/10.1149/1.3546038. http://jes.ecsdl.org/content/158/4/B416.abstract.

[30] Greszler TA, Caulk D, Sinha P. The impact of platinum loading on oxygen transport resistance. J Electrochem Soc 2012;159(12):F831–40. https://doi.org/10.1149/2.061212jes. http://jes.ecsdl.org/content/159/12/F831.abstract.

[31] Yoon W, Weber AZ. Modeling low-platinum-loading effects in fuel-cell catalyst layers. J Electrochem Soc 2011;158(8):B1007–18. https://doi.org/10.1149/1.3597644. http://jes.ecsdl.org/content/158/8/B1007.abstract.

[32] Singh R, Sui PC, Wong KH, Kjeang E, Knights S, Djilali N. Modeling the effect of chemical membrane degradation on pemfc performance. J Electrochem Soc 2018;165(6):F3328–36. https://doi.org/10.1149/2.0351806jes. http://jes.ecsdl.org/content/165/6/F3328.abstract.

[33] Lu L, Ouyang M, Huang H, Pei P, Yang F. A semi-empirical voltage degradation model for a low-pressure proton exchange membrane fuel cell stack under bus city driving cycles. J Power Sources 2007;164(1):306–14. https://doi.org/10.1016/j.jpowsour.2006.10.061. http://www.sciencedirect.com/science/article/pii/S037877530602146X.

[34] Zhang X, Yang D, Luo M, Dong Z. Load profile based empirical model for the lifetime prediction of an automotive PEM fuel cell. Int J Hydrog Energy 2017;42(16):11868–78. https://doi.org/10.1016/j.ijhydene.2017.02.146. http://www.sciencedirect.com/science/article/pii/S0360319917307139.

[35] Pei P, Chang Q, Tang T. A quick evaluating method for automotive fuel cell lifetime. Int J Hydrog Energy 2008;33(14):3829–36. https://doi.org/10.1016/j.ijhydene.2008.04.048. tMS07: Symposium on Materials in Clean Power Systems, http://www.sciencedirect.com/science/article/pii/S036031990800476X.
[36] Chen H, Pei P, Song M. Lifetime prediction and the economic lifetime of proton exchange membrane fuel cells. Appl Energy 2015;142:154–63. https://doi.org/10.1016/j.apenergy.2014.12.062. http://www.sciencedirect.com/science/article/pii/S0306261914013191.
[37] Mayur M, Strahl S, Husar A, Bessler WG. A multi-timescale modeling methodology for PEMFC performance and durability in a virtual fuel cell car. Int J Hydrog Energy 2015;40(46):16466–76. https://doi.org/10.1016/j.ijhydene.2015.09.152. http://www.sciencedirect.com/science/article/pii/S0360319915024829.
[38] Rinaldo SG, Stumper J, Eikerling M. Physical theory of platinum nanoparticle dissolution in polymer electrolyte fuel cells. J Phys Chem C 2010;114(13):5773–85. https://doi.org/10.1021/jp9101509. https://doi.org/10.1021/jp9101509.
[39] Hu X, Murgovski N, Johannesson LM, Egardt B. Optimal dimensioning and power management of a fuel cell battery hybrid bus via convex programming. IEEE ASME Trans Mechatron 2015;20(1):457–68. https://doi.org/10.1109/TMECH.2014.2336264.
[40] Hu X, Jiang J, Egardt B, Cao D. Advanced power-source integration in hybrid electric vehicles: multicriteria optimization approach. IEEE Trans Ind Electron 2015;62(12):7847–58. https://doi.org/10.1109/TIE.2015.2463770.
[41] Zheng C, Xu G, Park Y, Lim W, Cha S. Prolonging fuel cell stack lifetime based on Pontryagin's minimum principle in fuel cell hybrid vehicles and its economic influence evaluation. J Power Sources 2014;248:533–44. https://doi.org/10.1016/j.jpowsour.2013.09.110. http://www.sciencedirect.com/science/article/pii/S0378775313016169.
[42] Ahmadi P, Kjeang E. Realistic simulation of fuel economy and life cycle metrics for hydrogen fuel cell vehicles. Int J Energy Res 2017;41(5):714–27. https://doi.org/10.1002/er.3672. https://onlinelibrary.wiley.com/doi/abs/10.1002/er.3672.
[43] Hu Z, Li J, Xu L, Song Z, Fang C, Ouyang M, Dou G, Kou G. Multi-objective energy management optimization and parameter sizing for proton exchange membrane hybrid fuel cell vehicles. Energy Convers Manag 2016;129:108–21. https://doi.org/10.1016/j.enconman.2016.09.082. http://www.sciencedirect.com/science/article/pii/S0196890416308871.
[44] Fletcher T, Thring R, Watkinson M. An energy management strategy to concurrently optimise fuel consumption and PEM fuel cell lifetime in a hybrid vehicle. Int J Hydrog Energy 2016;41(46):21503–15. https://doi.org/10.1016/j.ijhydene.2016.08.157. http://www.sciencedirect.com/science/article/pii/S0360319916325435.
[45] Ramadass P, Haran B, Gomadam PM, White R, Popov BN. Development of first principles capacity fade model for Li-Ion cells. J Electrochem Soc 2004;151(2):A196–203. https://doi.org/10.1149/1.1634273. http://jes.ecsdl.org/content/151/2/A196.abstract.
[46] Wang J, Liu P, Hicks-Garner J, Sherman E, Soukiazian S, Verbrugge M, Tataria H, Musser J, Finamore P. Cycle-life model for graphite-LiFePO4 cells. J Power Sources 2011;196(8):3942–8. https://doi.org/10.1016/j.jpowsour.2010.11.134. http://www.sciencedirect.com/science/article/pii/S0378775310021269.
[47] Bowden FP. The influence of surface films on the friction, adhesion, and surface damage of solids. Ann N Y Acad Sci 1951;53(4):805–23. https://doi.org/10.1111/j.1749-6632.1951.tb54239.x. https://doi.org/10.1111/j.1749-6632.1951.tb54239.x.
[48] Darling RM, Meyers JP. Kinetic model of platinum dissolution in PEMFCs. J Electrochem Soc 2003;150(11):A1523–7. https://doi.org/10.1149/1.1613669. http://jes.ecsdl.org/content/150/11/A1523.abstract.
[49] NREL state-of-the-art fuel cell voltage durability status: 2016 composite data products. 05 2016. https://www.nrel.gov/docs/fy16osti/66581.pdf.
[50] Borup R, Davey J, Garzon F, Wood D, Welch P, More K. PEM fuel cell durability with transportation transient operation. ECS Trans 2006;3(1):879–86. https://doi.org/10.1149/1.2356206. http://ecst.ecsdl.org/content/3/1/879.abstract.
[51] Hu Z, Xu L, Li J, Ouyang M, Song Z, Huang H. A reconstructed fuel cell life-prediction model for a fuel cell hybrid city bus. Energy Convers Manag 2018;156:723–32. https://doi.org/10.1016/j.enconman.2017.11.069. http://www.sciencedirect.com/science/article/pii/S0196890417311214.
[52] Kim J, Kim M, Kang T, Sohn Y-J, Song T, Choi KH. Degradation modeling and operational optimization for improving the lifetime of high-temperature PEM (proton exchange membrane) fuel cells. Energy 2014;66:41–9. https://doi.org/10.1016/j.energy.2013.08.053. http://www.sciencedirect.com/science/article/pii/S0360544213007421.
[53] Bykolu A. Review of proton exchange membrane fuel cell models. Int J Hydrog Energy 2005;30(11):1181–212. https://doi.org/10.1016/j.ijhydene.2005.05.010. fuel Cells, http://www.sciencedirect.com/science/article/pii/S0360319905001898.
[54] O'hayre R, Cha S-W, Colella WG, Prinz FB. Fuel cell fundamentals. 3rd ed. John Wiley & Sons; 2016. https://app.knovel.com/hotlink/khtml/id:kt00CR5KS3/fuel-cell-fundamentals/a-1d-fuel-cell-model.
[55] Fowler MW, Mann RF, Amphlett JC, Peppley BA, Roberge PR. Incorporation of voltage degradation into a generalised steady state electrochemical model for a PEM fuel cell. J Power Sources 2002;106(1):274–83. https://doi.org/10.1016/S0378-7753(01)01029-1. proceedings of the Seventh Grove Fuel Cell Symposium, http://www.sciencedirect.com/science/article/pii/S0378775301010291.
[56] DOE fuel cell bus project. 2018. https://www.nrel.gov/hydrogen/fuel-cell-bus-evaluation.html.
[57] Perez HE, Hu X, Dey S, Moura SJ. Optimal charging of Li-Ion batteries with coupled electro-thermal-aging dynamics. IEEE Trans Veh Technol 2017;66(9):7761–70. https://doi.org/10.1109/TVT.2017.2676044.
[58] DOE. DOE technical targets for hydrogen production from electrolysis. 2011. https://www.energy.gov/eere/fuelcells/doe-technical-targets-hydrogen-production-electrolysis.
[59] DOE. DOE technical targets for fuel cell systems and stacks for transportation applications. 2015. https://energy.gov/eere/fuelcells/doe-technical-targets-fuel-cell-systems-and-stacks-transportation-applications.
[60] DOE. Overview of the DOE VTO advanced battery RD program. 2016. https://energy.gov/sites/prod/files/2016/06/f32/es000_howell_2016_o_web.pdf.
[61] Bertsekas DP. Dynamic programming and optimal control. 4th ed. Athena Scientific; 2017.